USING NANOPARTICLES FOR ENHANCING THE FOCUSING HEATING EFFECT OF AN EXTERNAL WAVEGUIDE APPLICATOR FOR ONCOLOGY HYPERTHERMIA: EVALUATION IN MUSCLE AND TUMOR PHANTOMS

C. J. Trujillo-Romero [1, *], S. García-Jimeno [2], A. Vera [1], L. Leija [1], and J. Estelrich [2, 3]

[1]Electrical Engineering Department, Bioelectronics Section, CINVESTAV-IPN, Mexico D.F., Mexico

[2]Departament de Fisicoquímica, Facultat de Farmàcia, Universitat de Barcelona, Avda. Joan XXIII, Barcelona 08028, Catalonia, Spain

[3]Institut de Nanociència i Nanotecnologia, IN[2]UB, Universitat de Barcelona, Spain

Abstract—A technical challenge in hyperthermia therapy is to locally heat the tumor region up to an appropriate temperature to destroy cancerous cells, without damaging the surrounding healthy tissue. Magnetic fluid hyperthermia (MFH) is a novel, minimally invasive therapy aiming at concentrating heat inside cancerous tissues. This therapy is based on the injection of different superparamagnetic nanoparticles inside the tumor. In our study, superparamagnetic nanoparticles, which we developed and characterized, consisted of iron oxide nanoparticles stabilized with polyethylene glycol. Moreover, a new technique for MFH using a specially designed external electromagnetic waveguide as applicator is presented. Three magnetite concentrations were used for making the tumor phantoms, which were embedded in muscle phantoms. The phantoms were radiated and located at three different distances from the applicator. Furthermore, two volumes of tumor (2.5 mL and 5.0 mL) were assayed. Heating curves, as a function of time, allowed the establishment of a more appropriate nanoparticle concentration for obtaining the temperature increase suitable for hyperthermia therapy. The results shown in this

paper confirm the feasibility of using nanoparticles as agents to focus the energy over the tumor, without creating hot spots in healthy tissue. In addition, the experiments validated that by using this applicator in combination with nanoparticles, it is also possible to locally control the increments of temperature in tissues.

1. INTRODUCTION

The biological effectiveness of heating for cancer treatment, so-called hyperthermia, has been known for decades [1, 2]. Hyperthermia, which is an increase of temperature up to $42°C$ to $45°C$, can be artificially induced by using drugs, particles, or medical devices [3, 4]. One kind of hyperthermia therapy is the magnetic fluid hyperthermia (MFH), which exploits the magnetic properties of nano-size iron oxides to destroy tumor cells; these nanoparticles might also be used as agents to enhance chemotherapy and radiotherapy [5, 6]. It has been shown that ferrofluid-mediated hyperthermia can be synergistically enhanced and improved by chemotherapy using magnetic nanoparticles functionalized with various anticancer drugs [7, 8]. The most used nano-size iron oxides are maghemite (γ-Fe_2O_3) and magnetite (Fe_3O_4). The reasons for this choice are: (i) both the iron oxides are biocompatible; (ii) they can be synthesized on a large scale; and (iii) their magnetization is significantly high, thus allowing these particles to be easily controlled by an external magnetic fields [9]. When magnetic nanoparticles are exposed to an appropriate AC magnetic field, the magnetic energy is converted into heat [10, 11]. The transformation of the magnetic energy into heat is due to the Néel relaxation, which is caused by the rapidly alternating magnetic dipole moments, and the Brownian relaxation, which is due to nanoparticle rotation, resulting in friction of the particles with the fluid [13]. For ferrofluids, which are stabilized magnetic nanoparticles, the Brownian and Néel relaxations depend on the particle size ($\sim$20 nm) [14]. If magnetic nanoparticles are inserted inside a tumor, as magnetic fields can penetrate the body, the application of an external electromagnetic (EM) field in the desired range of radiofrequencies will generate a thermal shock which will destroy the cells of the tumor without damaging the surrounding healthy tissues noninvasively. This is achieved by increasing the susceptibility of carcinogenic cells in environments of 42–45°C temperature, leading to apoptotic reactions [12]. The heat generated by the nanoparticles has a therapeutic effect similar to that obtained by conventional hyperthermia treatments but with the advantage that it is concentrated only at the tumor.

Nowadays, several studies concerning ferrofluid behavior in hyperthermia treatments have been performed by using coils to generate alternating magnetic fields, which excite nanoparticles implanted in tumors [15, 16]. Magnetic fields at low frequencies (e.g., 153 kHz) are used in most of the studies carried out in hyperthermia treatments [10]. Even if coils are the typical devices to generate alternating magnetic fields, there are other devices that are able to generate such fields, and one of them is the waveguide (WG).

In hyperthermia, WGs radiate EM waves into the patient. The TE mode is the most often used in hyperthermia treatments [17–19]. The TE waveguide primarily generates an electric field perpendicular to the propagation axes; the electrical field interacts with the dielectric properties of the tissue thereby causing heating. WGs also generate a magnetic field; however, the permeability of biological tissues is equal to that of free space, and, in consequence, biological tissues are considered for this application as nonmagnetic [20]. Hence, the magnetic field generated by the applicator cannot cause heating in the tissue. For this reason, hyperthermia studies carried out with WGs only took into account the electric field generated by the applicator.

At present, the use of magnetic nanoparticles as an agent to focus EM energy is one of the most promising techniques in hyperthermia. In this paper, we use magnetic nanoparticles coated with polyethylene glycol (PEG) as a system of nanoparticles for exploiting the magnetic field generated by a WG. PEG stabilizes the nanoparticles thereby avoiding aggregation and conferring biostability to them because the *in vivo* clearance of the nanoparticles is significantly delayed [15]. Because of their high flexibility and hydrophilicity, PEG macromolecules are good stabilizing agents. In the cited studies, the magnetic particles have been stabilized by substances different than PEG. According to our information, this is the first time that an unmodified PEG has been used to obtain a ferrofluid suitable for hyperthermia studies. In unpublished studies, we have checked the stability of ferrofluid performed with several amounts and molecular weights of PEG. The use of PEG 6000 afforded a material with a great stability. And, furthermore, the obtained ferrofluid is wholly biocompatible and biodegradable. The used concentration of magnetite is similar to that found in literature.The synergic use of a rectangular WG and magnetic nanoparticles allows taking advantage not only of the effect of the electric field but also of the effect of the magnetic field in a hyperthermia therapy. With this approach, the area of energy deposition can be locally controlled, thereby potentiating the heating effect in the tumor. On the other hand, it is also possible to reduce the time of treatment, as well as the input power used in the hyperthermia

treatment.

Nowadays, different equations describe the interaction of EM fields with tissue; this interaction causes heating in biological tissues. Bioheat transfer equation (BHTE) is used to describe the temperature evolution in biological tissues. The BHTE proposed by Pennes [21] can be written as:

$$\rho_t C_t \frac{\partial T}{\partial t} = \text{div}\,(k\nabla T) + \omega_b \rho_b C_b\,(T_b - T) + Q_{met} + Q_{ext}, \qquad (1)$$

where ρ_t, C_t, and k, are the density, specific heat and thermal conductivity of the tissue, respectively; ρ_b, C_b, and ω_b are the density, specific heat and perfusion rate of blood, respectively; T_b is the arterial blood temperature; Q_{met} is the heat source from metabolism, and Q_{ext} is the absorbed power density which can be written as:

$$Q_{ext} = \frac{1}{2}\sigma_t\,|E|^2, \qquad (2)$$

where σ_t is the electrical conductivity of the tissue and E is the electric field generated by the WG applicator. By analyzing Eq. (2), it is evident that only the E field is taken into account to achieve the temperature increase in tissues and tumors. Although the WG applicator generates E and H fields, the last one is neglected because tissues are considered in these studies as nonmagnetic. However, when magnetic nanopartices are injected into tumors, their magnetic properties are intensified, and consequently, the H field also is involved in the heating process.

On the other hand, if magnetic nanoparticles are concentrated inside tumors the absorbed power density is given by [22]:

$$Q_{ext} = \pi\mu_0\chi'' f H^2 \qquad (3)$$

where μ_0 is the permeability of free space, χ'' is the imaginary part of the magnetic susceptibility, f is the frequency of the alternating magnetic field, and H is the magnetic field amplitude. From Eq. (3), it is observed that temperature increments are proportional to the square of the amplitude of the H field intensity [20]. In which case, the E and H fields can be used as sources for heating, by substituting Eqs. (2) and (3) by Eq. (1), the BHTE can be rewritten in other terms as:

$$\rho_t C_t \frac{\partial T}{\partial t} = \text{div}\,(k\nabla T) + \omega_b \rho_b C_b\,(T_b - T) + Q_{met} + \frac{1}{2}\sigma_t|E|^2 + \pi\mu_0\chi'' f H^2 \quad (4)$$

From Eq. (4), it can be observed that the heating effect is produced by both the electric and magnetic fields generated by the external applicator; i.e., the heating effect produced by the WG applicator depends not only of the square of E field but also of the square of

H field. For this reason, the heating efficiency is higher compared with that obtained with a coil; in which just the magnetic field is taken into account for heating. In this sense, to test the hyperthermic effect of magnetic nanoparticles, and to observe the behavior of temperature increase in the deep regions and the dependence of the concentration of magnetic particles in the tumor tissue, the distribution of temperature increases, along the depth of agarose phantoms with different concentrations of magnetic particles, has been analyzed.

2. MATERIALS AND METHODS

2.1. Materials

All chemicals were of reagent grade and used without purification. Ferric chloride hexahydrate ($Cl_3Fe.6H_2O$) and ferrous chloride tetrahydrate ($Cl_2Fe.4H_2O$) were purchased from Sigma-Aldrich (St. Louis, MO). Agarose (Ultrapure^{TM} agarose) was purchased from Invitrogen (Mexico, D.F.). Polyethylenglycol (PEG) of 6000 Da molecular weight was from VWR International (Barcelona, EU). Ammonium hydroxide (NH_4OH, 25%) was from Panreac (Barcelona, EU). Deionized Millipore Milli-Q water was used in all experiments. A strong neodymium — iron — boron ($Nd_2Fe_{12}B$) magnet (1.2 T) was obtained from Halde GAC (Barcelona, EU).

2.2. Synthesis and Characterization of Ferrofluid

The ferrofluid was prepared by using a co-precipitation method in the presence of excess PEG. Briefly, once the polymer was dissolved in water, $FeCl_2/FeCl_3$ at $1:2$ molar ratio were added. When the PEG and iron salts were well dissolved, a 25% (v/v) NH_4OH solution was added with vigorous mechanical stirring. Later, the ferrofluid was poured into a beaker and the vessel was placed onto the permanent magnet. The ferrofluid was washed four times with water by decanting the supernatant so as to eliminate excess PEG. Finally, water was added until the desired concentration was obtained. The final suspension was sonicated (Transsonic Digital Bath sonifier, Elma, EU). The morphology of the ferrofluid was studied by transmission electron microscopy (TEM_i) by using a Jeol 1010 microscope at an accelerating voltage of 80 kV. Images were recorded with a Megaview III camera. The acquisition was accomplished with Soft-Imaging software (SIS, EU). Samples were prepared by deposition of one drop of an appropriately diluted solution onto a copper grid coated with carbon film with a Formvar membrane and drying it in air before it was loaded onto the microscope. The hydrodynamic diameter of the

magnetic particles was determined by dynamic light scattering at $90°$ with a Zetasizer Nano (Malvern, EU) at $25°$C. The Fe_3O_4 content of ferrofluid was determined by a colorimetric method based on the titration of ferrous ion by o-phenanthroline. Magnetic measurements were made in a superconducting quantum interference device (SQUID) magnetometer (Quantum design MPMS XL) at room temperature. The external magnetic field was swept from $+5,000$ to $-5,000$ Oe, and then back to $+5,000$ Oe.

2.3. Agarose Muscle and Tumor Phantoms with Different Concentrations of Ferrofluid

2.3.1. Solid Muscle Phantom

A phantom based on agarose (17.8 g), tri-distilled water (1 L), ethanol (1 L), and NaCl (12 g) [23] was made to simulate the relative permittivity and electrical conductivity [24, 25] of muscle tissue at 224 MHz (the work frequency of the RF applicator). Muscle relative permittivity, reported in the literature at 224 MHz, is 60.7 and electrical conductivity is 0.743 S/m. Tri-distilled water, ethanol, and NaCl were mixed and heated at $\sim80°$C. When this mixture reached $80°$C, agarose was added and it was totally dissolved. The final mixture was poured into a special methacrylate container. Phantom permittivity was measured by using a dielectric probe kit (85070C, Hewlett Packard, USA), whereas the electrical conductivity was obtained by means of Eq. (5)

$$\sigma = \varepsilon'' \varepsilon_0 \omega \tag{5}$$

where σ is the electrical conductivity, ε'' is the loss factor, ε_0 is the permittivity of free space, and $\omega = 2\pi f$ is the angular frequency. The final volume of muscle phantom was approximately 2.85 L.

2.3.2. Tumor and Ferrofluid Concentration

The ferrofluid was concentrated in small spheres of agarose (~18 mm diameter). Each sphere was made with 0.006 g/mL of agarose and several amounts of ferrofluid. Such spheres simulated a cancerous tissue, a carcinoma in this case. Permittivity of carcinomas at 224 MHz is 59, and its electrical conductivity 0.9 [25, 26]. Two sizes of spheres were used: 2.5 mL and 5.0 mL. For the spheres of 2.5 mL, three different concentrations of ferrofluid were used: 4.4 mg/mL, 8.8 mg/mL, and 13.3 mg/mL of magnetite. These spheres were introduced inside the muscle phantom at 2 cm, 3 cm and 4 cm depths before it was totally solidified. For the spheres of 5 mL, which mimic bigger tumors, only one concentration of ferrofluid (8.8 mg/mL of magnetite) was used.

2.4. RF WG Applicator

The applicator is a radiofrequency (RF) WG which works in TE_{10} mode ($m = 1$, $n = 0$) [27]. TE_{10} is a dominant propagation mode, i.e., only one wave travels inside the WG. To propagate only the TE_{10} mode, the WG dimensions must be calculated at a specific
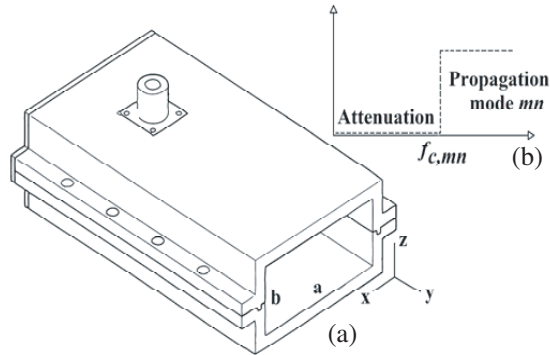
Figure 1. (a) x-, y-, and z-axes of a rectangular WG and WG apertures a and b. (b) TE_{mn} propagation mode due to the cutoff frequency.
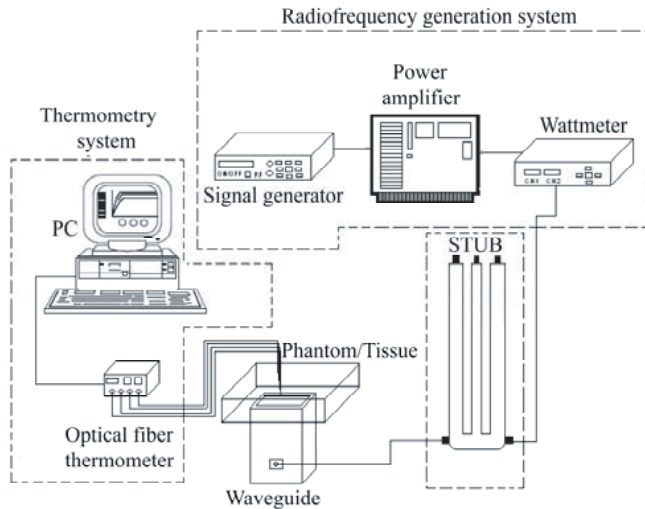
**Figure 2.** The experimental setup needed to carry out the thermal tests.

cutoff frequency. The cutoff frequency assures that waves at other low frequencies cannot propagate inside the WG as is depicted in Fig. 1(b). This applicator was specially designed to work at 224 MHz; its dimensions were $a = 7.9$ cm and $b = 3.9$ cm (Fig. 1(a)).

2.5. RF System

The RF system consists of a radiofrequency generation system comprising a signal generator (SML03, Rohde&Schwartz, Germany), a power amplifier (500A250, Amplifier Research, USA), and a power meter (PM2002, Amplifier Research, USA). Finally, so as to match the RF system with the applicator, a stub (matching coupler) was used. Fig. 2 shows the complete experimental setup for inducing and measuring the temperature increase.

2.6. Temperature Measurements

Four non-EM interfering temperature sensors (M3300, Luxtron, USA), based on optical fiber, were used to record temperature increases. These temperature measurements were recorded inside the muscle phantom and ferrofluid, just above the central point of the aperture of the applicator (Fig. 3). The input power used in each test was 66 W. Each tests lasted 960 s; this time was chosen in order to study the response as a function of time and to simulate more real conditions.
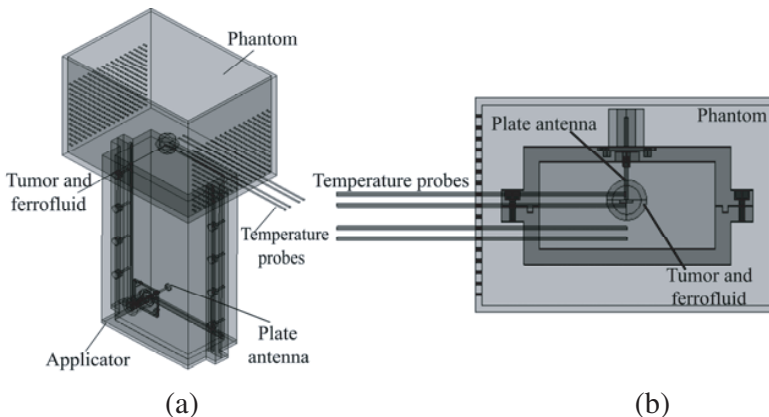

Figure 3. Experimental setup to measure temperature increments inside the muscle phantom and the tumor. (a) Tridimensional view of the setup. (b) Top view of the setup.

Optical fiber sensors were chosen because they do not modify the radiation pattern of the applicator. One sensor was placed approximately at the center of the sphere (tumor); another one was placed at 0.5 cm from the first sensor (inside the tumor). Finally, both remaining sensors were placed at 1.5 cm and 2 cm from the first sensor, respectively. The last two sensors were placed outside the ferrofluid (when spheres of 2.5 mL were used). For the spheres of 5.0 mL, only the sensor at 2 cm was out of the tumor, just in contact with the muscle phantom. The final phantom (muscle and tumor phantom) was irradiated for 20 min; at 16 min all sensors were displaced by 0.5 cm, and after every 30 s they were displaced to cover a distance of 4 cm at one side. Temperature experiments were recorded at 2 cm, 3 cm and 4 cm depths, where the spheres (tumor and ferrofluid) were placed so as to simulate tumors at different depths; this analysis was carried out to know the viability of our applicator to treat tumors localized at different depths. The initial temperature of the muscle phantom was controlled at 25°C. The radiation was applied five times to all the phantoms and the temperatures were acquired every second during the experiments using True Temp software (Luxtron, USA).

3. RESULTS AND DISCUSSION

3.1. Synthesis and Characterization of Ferrofluid

Figure 4 shows a transmission electron microscopy (TEM_i) micrograph from which the spherical shape and an average diameter of 15 nm of the particles of ferrofluid were observed. The z-average diameter of particles obtained by dynamic light scattering was 51.7 nm $\pm$ 1.2 nm; this value was much larger than that found from TEM_i. This was because even in the absence of any external magnetic field, the magnetostatic (magnetic dipole-dipole) interactions among the particles can cause their agglomeration. The particle size distribution was designated by the polydispersity index (PI) (0.181 ± 0.003), which varied from 0.0 for an entirely monodisperse sample to 1.0 for a polydisperse sample. The Fe_3O_4 concentration of ferrofluid determined spectrophotometrically was 22 mg/mL. The magnetic hysteresis loop of the ferrofluid measured at room temperature is shown in the inset of Fig. 4. The saturation magnetization of magnetic nanoparticles was about 52 emu/g, and the coercive field was closed to zero. This means that the sample exhibited superparamagnetic behavior and had high magnetization that determines the heating power in magnetic heating experiments.
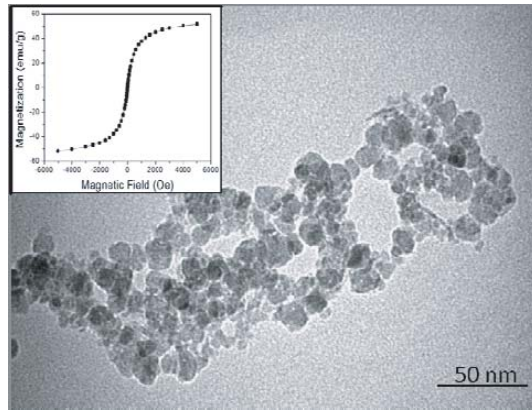
Figure 4. TEM$_i$ image of the ferrofluid used in the experiment. Inset: magnetization curve for ferrofluid as a function of the applied magnetic field.

Table 1. Dielectric properties of muscle, carcinoma, and their equivalent phantoms.

Dielectric properties	Muscle tissue (literature)	Carcinoma (literature)	Muscle phantom (measured)	Carcinoma phantom (measured)
Relative permittivity	60.70	~59.00	61.13 ± 0.98	62.80 ± 2.00
Electrical conductivity (S/m)	0.74	~0.90	0.50 ± 0.03	0.52 ± 0.06

3.2. Agarose Muscle and Cancer Tumor Phantoms with Various Concentrations of Ferrofluid

For the developed phantoms (Fig. 5), their relative permittivity and electrical conductivity have to be similar to that of the tissues the phantoms mimic. Table 1 shows the values for the dielectric properties of muscle and carcinomous tissues (obtained from the literature) [23, 26] as well as the experimentally measured values in our phantoms. As can be seen, dielectric properties achieved in the muscle phantom showed similar values to those reported in the literature; the differences in the relative permittivity and conductivity observed between phantoms and carcinomas were 3.8 units and 0.375 S/m, respectively.
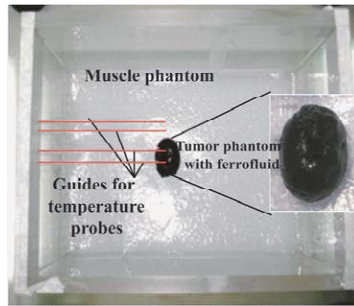
Figure 5. Muscle and carcinoma phantoms; the latter contains the ferrofluid.

3.3. Temperature Measurements

Figure 6 depicts the time-dependent temperature increments obtained for each of the three different concentrations of magnetite analyzed. Fig. 6(a) shows the temperature behavior for a concentration of 4.4 mg/mL of magnetite when the tumor phantom is located at 2 cm, 3 cm and 4 cm depths from the WG. When the tumor phantom was located at 2 cm, the temperature increment recorded by the probe inserted in the middle point of the tumor was approximately 10°C, whereas the other probes recorded lower increments of temperature. The temperature difference between the probe inside the tumor and the one located 2 cm away from the middle was 2.7°C; this means that the heat is concentrated inside the tumor. As a general rule, the increases in temperature were progressively smaller with the depth increasing. At 3 cm depth, the increase of temperature recorded by the central probe was ∼7°C and, at the same depth, but 2 cm away, the increase was just ∼4°C. From Fig. 6, it can be concluded that at 2 cm and 3 cm depths, the obtained increments can be considered within the therapeutic hyperthermia range (∼7°C), whereas the heating at 4 cm depth reached only an increment of 2°C.

Figures 6(b) and (c) show the temperature tendency as a function of time for 8.8 mg/mL and 13.3 mg/mL of magnetite, respectively. The concentration of 8.8 mg/mL shows that when the tumor is at 2 cm depth (red lines), the obtained heating is similar over the whole tumor because the difference of temperature is only 0.22°C between the probe located in the inner and that at 0.5 cm, whereas the differences with the other sensors were 2.5°C and 5°C, respectively. Finally, Fig. 6(c) shows that a concentration of 13.3 mg/mL of magnetite tends to saturation; that is, the amount of magnetite is higher than the maximum concentration which can be excited by the magnetic
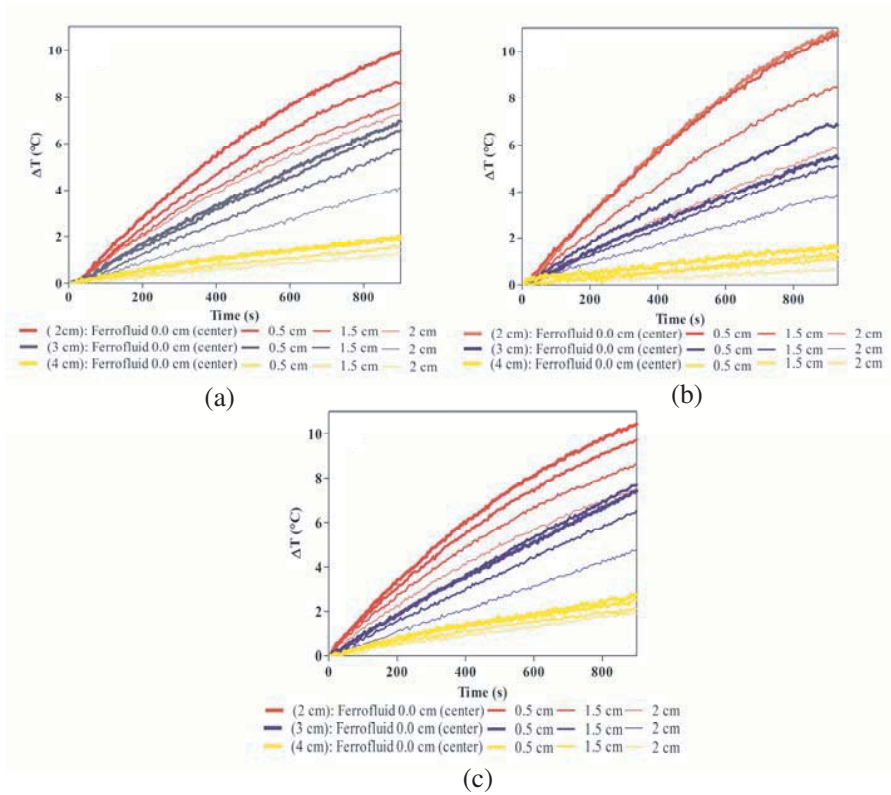
Figure 6. Temperature increments obtained with. (a) 4.4 mg/mL of magnetite. (b) 8.8 mg/mL of magnetite. (c) 13.3 mg/mL of magnetite. For each concentration, 12 time-dependent curves are displayed. They can be grouped in three series, each one indicated by a different color: red lines represent the temperature increments when the tumor is at 2 cm depth from the applicator; blue lines when the tumor is at 3 cm depth; and yellow lines when it is at 4 cm depth. For each tumor at a determined depth, the temperature was determined at the center of the tumor phantom, at 0.5 cm from the center (but still inside the tumor), and at 1.5 cm and 2.0 cm from the center (both outside the tumor).

field generated by the WG applicator. As a consequence, though the concentration of magnetite is higher, the temperature increments achieved were similar to those obtained with a concentration of 8.8 mg/mL of magnetite.

Table 2 summarizes the temperature increments recorded at the end of each test. As can be observed, the three concentrations of

Table 2. Maximum temperature increment obtained at the end of the tests (960 s) with each concentration of ferrofluid at 2 cm, 3 cm and 4 cm depths.

Ferrofluid concentration (mg/mL)	$\Delta T (^{\circ}C)$ Probe 1 (inside the tumor)	$\Delta T (^{\circ}C)$ Probe 2 (0.5 cm inside the tumor)	$\Delta T (^{\circ}C)$ Probe 3 (1.5 cm outside the tumor)	$\Delta T (^{\circ}C)$ Probe 4 (2 cm outside the tumor)
4.4 at 2.0 cm	10.20	8.94	7.28	7.49
4.4 at 3.0 cm	7.18	6.90	5.83	4.35
4.4 at 4.0 cm	2.05	2.13	1.64	1.22
8.8 at 2.0 cm	11.14	10.92	8.65	6.06
8.8 at 3.0 cm	4.65	5.78	4.18	3.21
8.8 at 4.0 cm	1.68	1.36	1.20	0.72
13.3 at 2.0 cm	11.11	10.20	9.07	7.59
13.3 at 3.0 cm	7.80	8.13	6.87	5.11
13.3 at 4.0 cm	2.90	2.62	2.28	2.10

ferrofluid reached a temperature increase suitable for hyperthermia therapy when the tumor was at 2 cm from the applicator. In contrast, the temperature increments are lower in the case where the tumor was at 4 cm depth ($\sim$3°C). Concerning the 4.4 mg/mL concentration, at 3 cm depth, the heat was more concentrated inside the tumor, because the temperature difference between both probes in the tumor was 0.28°C, whereas temperature differences with the other probes outside the tumor were 1.35°C and 2.83°C, respectively. The concentration of 8.8 mg/mL at 2 cm depth shows a high capacity of focusing heat. In this way, the temperature difference inside the tumor was 0.22°C, whereas temperature differences with the other probes were 2.49°C and 5.08°C; that is, at 2 cm away from the tumor, the temperature decreased approximately by 5°C. For a concentration of 13.3 mg/mL (at 2 cm depth), the temperature difference inside the tumor was 0.91°C whereas with the other probes were 2.04°C and 3.52°C, respectively. Finally, at 3 cm depth, the temperature difference in the tumor was 0.28°C and temperature differences with the other probes were 1.26°C and 3.02°C, respectively. In conclusion, each concentration presented a tendency to localize temperature rise within the tumor. These results were corroborated by the thermograms shown

in Figs. 7(a) and 7(e); here, the temperature distributions obtained without ferrofluid are shown. The uniform temperature distribution generated by the WG is not concentrated just over the tumor phantom (agarose with ferrofluid), while in the other case, when we use the ferrofluid, the heat was concentrated inside the tumor (See Figs. 7(b)–(d) and Figs. 7(f)–(h).

Figures 7(a)–(l) depict the thermal distributions obtained with each concentration of magnetite. From these figures the focusing effect produced by the ferrofluid could be observed. Figs. 7(a)–(d) show the temperature distributions for 4.4 mg/mL, 8.8 mg/mL, and 13.3 mg/mL of the magnetite when the tumor was located at 2 cm depth, and the temperature distributions in the absence of magnetite, 0.0 mg/mL. Such temperature distributions clearly demonstrate the focusing effect of the heat produced by the ferrofluid. As observed in Fig. 7(a), in a muscle phantom without ferrofluid, the surface that presented temperature increments of at least 7°C, which is needed to induce hyperthermia, was of approximately 3 cm × 4 cm; that is to say, the temperatures reached in this area were suitable for hyperthermia therapy. The highest temperatures were measured at the center of the WG aperture (in each figure, the gray dashed line represents the aperture of the applicator). The shapes of the temperature distributions changed when the concentration of magnetite in the ferrofluid varied. For 4.4 mg/mL of the magnetite (if the tumor is at 2 cm depth) (Fig. 7(b), the therapeutic heating area was approximately 2 cm × 2 cm with a maximum increment of 9.37°C. In the temperature distribution obtained with 8.8 mg/mL (Fig. 7(c)), the therapeutic heating region was approximately 1 cm × 3 cm with a maximum increment of 9.43°C, whereas for a distribution with 13.3 mg/mL (Fig. 7(d)) this region was quite bigger, 2 cm × 4 cm, and the increment achieved was 8.49°C. By analyzing these results, dependence among the concentrations of magnetite, temperature, and size of the heating region was observed. It is true that for a concentration of 13.3 mg/mL of magnetite, the temperature achieved was lower than for that obtained with 8.8 mg/mL, but, as previously noted, the amount of magnetite is higher than that which can be excited by the applicator. Of the three concentrations, the optimal results were obtained with the concentration of 8.8 mg/mL of magnetite, because the temperature achieved was the highest, and the generated therapeutic heating area was focused in a small region, just inside the tumor.

Figures 7(e)–(h) show the temperature distributions for the mentioned concentrations but at 3 cm depth. In a muscle phantom without ferrofluid, the area of the therapeutic heating region was approximately 3 cm × 4 cm and the temperature increment achieved
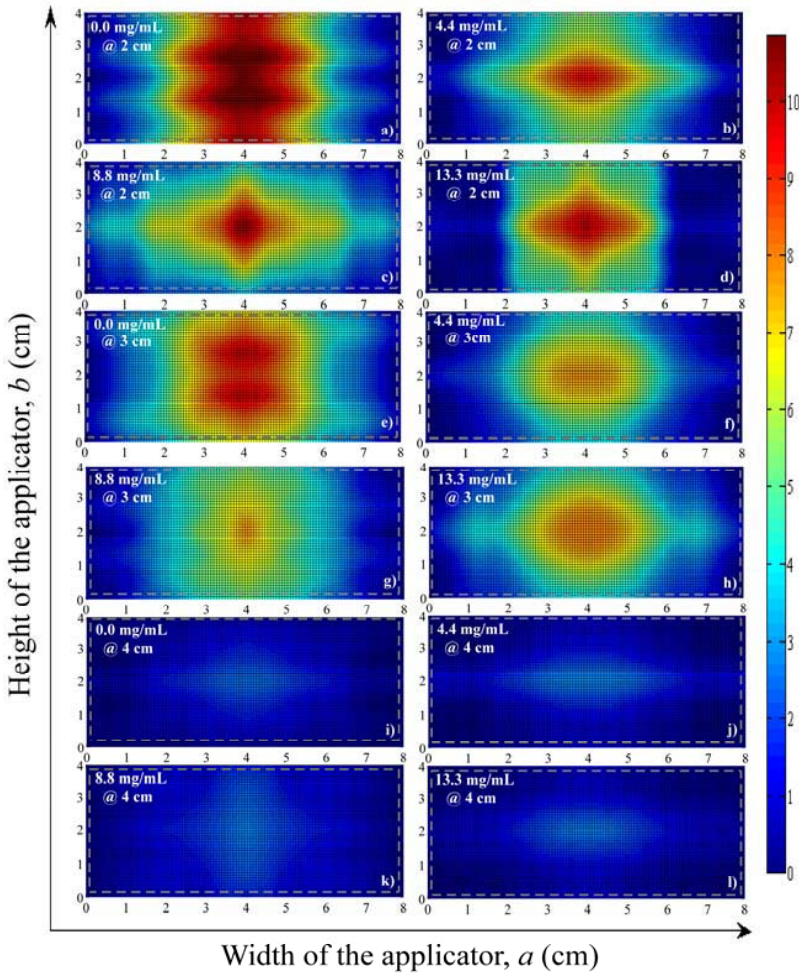
Figure 7. Thermograms obtained after applying the EM radiation on a muscle phantom containing a carcinoma phantom, whose volume is 2.5 mL, at several depths (Figs. 4(a)–(d), 2 cm; Figs. 4(e)–(h), 3 cm; Figs. 4(i)–(l), 4 cm). The carcinoma phantom contained the following concentrations of magnetite: 0.0 mg/mL (Figs. 4(a), (e), (i), 4.4 mg/mL.) (Figs. 4 (b), (f), (j), 8.8 mg/mL.) (Figs. 4(c), (g), (k), and 13.3 mg/mL.) (Figs. 4(d), (h), (l). On the right, the color scale of temperature increments.)

(a)   (b)
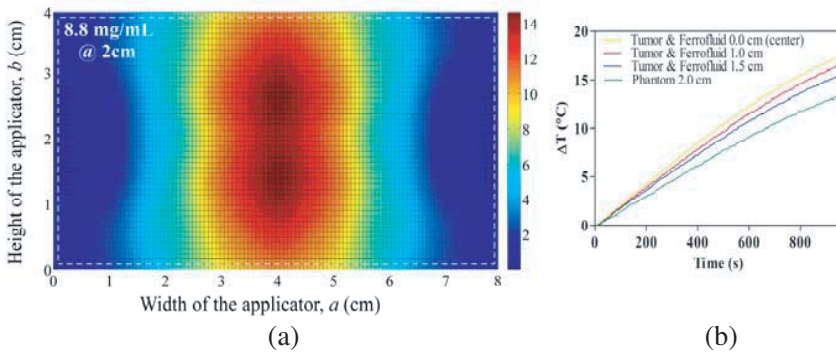
Figure 8. Temperature increments obtained for a tumor phantom
with a volume of 5 mL. (a) Temperature distributions obtained at 2 cm
depth with a concentration of 8.8 mg/mL magnetite. (b) Temperature
increments obtained with 8.8 mg/mL of magnetite. Probes 1, 2, and
3 are inside the tumor, whereas probe 4 is just in contact with the
muscle phantom.

was 9.8°C (Fig. 7(e)). A therapeutic heating region of ~2.5 cm ×
2 cm and a temperature increment of 7.7°C were obtained when
the carcinoma contained magnetite at a concentration of 4.4 mg/mL
(Fig. 7(f)). The thermal distribution obtained with 13.3 mg/mL
showed a therapeutic heating region of approximately 3 cm × 3 cm
and the maximum temperature achieved was 8.3°C (Fig. 7(h)). The
concentration of 8.8 mg/mL provided a rather special distribution of
heating (Fig. 7(g)); the pattern of the distribution of temperatures
showed a small focus of heat with a maximum temperature increment
of 8.1°C. The therapeutic heating region, 1 cm × 4 cm, was smaller
than that obtained with other conditions. This singular effect was
observed repeatedly in all the analyzed samples. Finally, temperature
distributions at 4 cm depth obtained with each concentration of
magnetite are shown in Figs. 7(i)–(l). As observed previously (Fig. 6),
at this depth, the temperature increments were not enough elevated
to produce hyperthermia effects. However, the heat focusing effect
of the ferrofluid over the tumor was clearly visible (we can observe
a light blue color at the center of the thermogram, corresponding to
increments of 3–4°C, on a dark blue color, which comprises increments
of temperature only up to 1°C). Table 3 summarizes the heating
area and the maximal increment of temperature achieved with each
concentration at each analyzed depth.

Table 3. Area comprising the increments of temperature higher than 7°C (therapeutic temperature) and the maximal temperature increments achieved.

Concentration of magnetite (mg/mL)	Therapeutically useful area	Maximal temperature increment (°C)
0.0 at 2.0 cm	3.0 cm × 4.0 cm	10.8°C.
4.4 at 2.0 cm	2.0 cm × 2.0 cm	9.4°C
8.8 at 2.0 cm	1.0 cm × 3.0 cm	9.4°C
13.3 at 2.0 cm	2.0 cm × 4.0 cm	8.5°C
0.0 at 3.0 cm	3.0 cm × 4.0 cm	9.8°C
4.4 at 3.0 cm	2.5 cm × 3.0 cm	7.7°C
8.8 at 3.0 cm	1.0 cm × 4.0 cm	8.1°C
13.3 at 3.0 cm	3.0 cm × 3.0 cm	8.3°C
0.0 at 4.0 cm	-	2.7°C
4.4 at 4.0 cm	-	2.9°C
8.8 at 4.0 cm	-	2.9°C
13.3 at 4.0 cm	-	2.9°C

To determine the influence of the size of the tumor on the temperature distribution, a tumor with a volume of 5 mL was used. The tumor contained ferrofluid of 8.8 mg/mL and it was located at 2 cm depth. Fig. 8(a) shows the obtained thermal distribution, where a maximal increment of 14.60°C was observed. In this case, the area with a minimal temperature increment of 7°C was approximately 3 cm × 4 cm. Here, we can observe that the heated area was dependent on the mass occupied by the ferrofluid. Fig. 8(b) shows the temperature increments as function of time. Due to the higher size of the tumor, now, probes 1, 2, and 3 recorded temperatures inside the tumor, whereas probe 4 recorded the temperature inside the muscle phantom. Temperature differences among probe 1, and probes 2 and 3 were 0.99°C and 2.1°C, respectively, and between probe 1 and probe 4 was 4.21°C. These differences show that the heat was concentrated especially inside the tumor.

4. CONCLUSION

A technical challenge in hyperthermia treatment is to locally heat the tumor region up to the appropriate therapeutic temperature without damaging the surrounding healthy tissue. This paper presents a study concerning the heating and focusing effect of the combination of a radiofrequency applicator (RF WG) and a ferrofluid as an alternative to focus the EM energy over a localized zone of the body. In our experiments, the EM energy is transformed into heat which leads to an increase of temperature; any increase equal or higher than $7°C$ is considered as suitable for hyperthermia therapy. The RF applicator used in this work generates electric and magnetic fields; the electric field interacts with the electrical properties of tissue, i.e., permittivity and conductivity. The magnetic properties of the tissue are extremely weak, the presence of superparamagnetic nanoparticles used in this work permits that, through the interaction of magnetic components of nanoparticles and radiation, an additional amount of heat is generated, i.e., the nanoparticles act as enhancers of the heating effect of our RF applicator.

The results shown in this paper confirm that the use of nanoparticles as agents to localized temperature rise in the whole tumor volume is feasible. Hence, by using this applicator in combination with nanoparticles it is possible: (i) to focus the energy over the tumor without creating hot spots in healthy tissue (the therapeutic region is determined by the volume occupied by the ferrofluid), (ii) to provide higher temperatures to tissues depending on the ferrofluid concentration (this fact is an advantage because the power used by the hyperthermia system could be reduced), and (iii) to control the increments of temperatures in tissues. We also found that there is a maximum magnetite concentration that the magnetic field, generated by the applicator, can excite; this concentration determines the maximum temperature reached inside the tumor phantom. On the other hand, from this study it can be concluded that the amount of magnetic nanoparticles which should be injected to obtain suitable thermal levels will depend on the depth and size of the tumor. Finally, we conclude that it is possible to use higher power inputs and reduce the radiation time or to use lower power inputs and increase radiation time.

ACKNOWLEDGMENT

REFERENCES

1. Falk, M. H. and R. D. Issels, "Hyperthermia in oncology," *International Journal of Hyperthermia*, Vol. 17, 1–18, Jan. 2001.

2. Hildebrandt, B., P. Wust, O. Ahlers, et al., "The cellular and molecular basis of hyperthermia," *Crit. Rev. Oncology/Hematology*, Vol. 43, 33–56, Jul. 2002.

3. Gupta, R. C. and S. P. Singh, "Elliptically bent slotted waveguide conformal focused array for hyperthermia treatment of tumors in curved region of human body," *Progress In Electromagnetics Research*, Vol. 62, 107–125, 2006.

4. Gong, Y. and G. Wang, "Superficial tumor hyperthermia with flat left-handed metamaterial lens," *Progress In Electromagnetics Research*, Vol. 98, 389–405, 2009.

5. Arruebo, M., R. Fernádez-Pacheco, M. R. Ibarra, and J. Santamaría, "Magnetic nanoparticles for drug delivery," *Nano Today*, Vol. 2, No. 3, 22–32, 2007.

6. Pankhurst, Q. A., J. Connolly, S. K. Jones, and J. Dobson, "Applications of magnetic nanoparticles in biomedicine," *Journal of Physics D: Applied Physics*, Vol. 36, No. 13, 167, 2003.

7. Babincová, M., P. Čičanec, V. Altanerová, C. Altaner, and P. Babinec, "AC-magnetic field controlled drug release from magnetoliposomes: Design of a method for site-specific chemotherapy," Bioelectrochemistry, Vol. 55, No. 1–2, 17–19, 2002.

8. Babincová, M., V. Altanerova, C. Altaner, C. Bergemann, and P. Babinec, "In vitro analysis of cisplatin functionalized magnetic nanoparticles in combined cancer chemotherapy and electromagnetic hyperthermia," *IEEE Transactions on Nanobioscience*, Vol. 7, No. 1, 15–19, 2008.

9. Luong, T. T., T. P. Ha, L. D. Tran, M. H. Do, T. T. Mai, N. H. Pham, H. B. T. Phan, G. H. T. Pham, N. M. T. Hoang, Q. T. Nguyen, and P. X. Nguyen, "Design of carboxylated fe3o4/poly(styrene-co-acrylic acid) ferrouids with highly efficient magnetic heating effect," *Colloids and Surfaces A: Physicochemical and Engineering Aspects*, Vol. 384, No. 1–3, 23–30, 2011.

10. Hiergeist, R., W. Andra, N. Buske, R. Hergt, I. Hilger, U. Richter, and W. Kaiser, "Application of magnetite ferrouids

for hyperthermia," *Journal of Magnetism and Magnetic Materials*, Vol. 201, 420–422, 1999.

11. Duguet, E., S. Vasseur, S. Mornet, and J.-M. Devoisselle, "Magnetic nanoparticles and their applications in medicine," *Nanomedicine*, Vol. 1, No. 2, 157–168, 2006.

12. Thomas, L. A., L. Dekker, M. Kallumadil, P. Southern, M. Wilson, S. P. Nair, Q. A. Pankhurst, and I. P. Parkin, "Carboxylic acid-stabilised iron oxide nanoparticles for use in magnetic hyperthermia," *J. Mater. Chem.*, Vol. 19, 6529–6535, 2009.

13. Laurent, S., D. Forge, M. Port, A. Roch, C. Robic, L. Vander Elst, and R. N. Muller, "Magnetic iron oxide nanoparticles: Synthesis, stabilization, vectorization, physicochemical characterizations, and biological applications," *Chemical Reviews*, Vol. 108, No. 6, 2064–2110, 2008.

14. Rovers, S. A., R. Hoogenboom, M. F. Kemmere, and J. T. F. Keurentjes, "Relaxation processes of superparamagnetic iron oxide nanoparticles in liquid and incorporated in poly(methyl methacrylate)," *The Journal of Physical Chemistry C*, Vol. 112, No. 40, 15643–15646, 2008.

15. Ingrid, H., et al., "Magnetic nanoparticles for selective heating of magnetically labelled cells in culture: preliminary investigation," *Nanotechnology*, Vol. 15, 1027, 2004.

16. Rudolf, H., et al., "Magnetic particle hyperthermia: Nanoparticle magnetism and materials development for cancer therapy," *J. Phys.: Condens. Matter*, Vol. 18, 2919, 2006.

17. Wiersma, J. and J. D. V. Dijk, "RF hyperthermia array modelling; validation by means of measured em-field distributions," *International Journal of Hyperthermia*, Vol. 17, No. 1, 63–81, 2001.

18. Nilsson, P., T. Larsson, and B. Persson, "Absorbed power distributions from two tilted waveguide applicators," *International Journal of Hyperthermia*, Vol. 1, No. 1, 29–43, 1985.

19. Gardner, R., H. Vargas, J. Block, C. Vogel, A. Fenn, G. Kuehl, and M. Doval, "Focused microwave phased array thermotherapy for primary breast cancer," *Annals of Surgical Oncology*, Vol. 9, 326–332, 2002.

20. Durney, C., C. Johnson, P. Barber, H. Massoudi, M. Iskander, S. Allen, and J. Mitchell, *Radiofrequency Radiation Dosimetry Handbook*, USAF School of Aerospace Medicine, 1986.

21. Pennes, H. H., "Analysis of skin, muscle and brachial arterial blood temperatures in the resting normal human forearm," *Am.*

J. Med. Sci., Vol. 215, No. 3, 354, 1948.

22. Skumiel, A., A. Jozefczak, M. Timko, P. Kopcansky, F. Herchl, M. Koneracka, and T. N., "Heating effect in biocompatible magnetic fluid," *International Journal of Thermophysics*, Vol. 28, No. 5, 1461–1469, 2007.

23. Gabriel, C., "Compilation of the dielectric properties of body tissues at RF and microwave frequencies," Report N.AL/OE-TR-1996-0037, Occupational and environmental health directorate, Radiofrequency Radiation Division, Brooks Air Force Base, Texas, USA, Jun. 1996.

24. Iero, D., T. Isernia, A. F. Morabito, I. Catapano, and L. Crocco, "Optimal constrained field focusing for hyperthermia cancer therapy: A feasibility assessment on realistic phantoms," *Progress In Electromagnetics Research*, Vol. 102, 125–141, 2010.

25. Lai, J. C. Y., C. B. Soh, E. Gunawan, and K. S. Low, "Homogeneous and heterogeneous breast phantoms for ultra-wideband microwave imaging applications," *Progress In Electromagnetics Research*, Vol. 100, 397–415, 2010.

26. Yoo, D.-S., "The dielectric properties of cancerous tissues in a nude mouse xenograft model," *Bioelectromagnetics*, Vol. 25, 492–497, 2004.

27. Trujillo-Romero, C. J., L. Leija, and A. Vera, "FEM modeling for performance evaluation of an electromagnetic oncology deep hyperthermia applicator when using monopole, inverted T, and plate antennas," *Progress In Electromagnetics Research*, Vol. 120, 99–125, 2011.